Glycosylated nanoparticles derived from RAFT polymerization for effective drug delivery to macrophages

James L. Rushworth,[†, ‡] Katherine S. Montgomery,[†, ‡] Benjamin Cao,[‡, §] Robert Brown,[⊥] Nick J. Dibb,[⊥] Susan K. Nilsson, [‡, §] John Chiefari[‡] and Matthew J. Fuchter*[†]

[†]Molecular Sciences Research Hub, Department of Chemistry, Imperial College London, White City Campus, London, UK, W12 0BZ.

Email: m.fuchter@imperial.ac.uk

[‡]CSIRO Manufacturing, Bag 10, Clayton South MDC, Victoria 3169, Australia

[§]Australian Regenerative Medicine Institute, Monash University, Clayton, Victoria 3800, Australia.

[⊥]Department of Surgery & Cancer, Imperial College London, London, UK, SW7 2AZ

Keywords: Drug delivery; macrophages; tumor-associated macrophages; CD206; mannose; glycopolymers.

ABSTRACT: The functional-group tolerance and simplicity of reversible addition fragmentation chain transfer (RAFT) polymerization enables its use in the preparation of a wide range of functional polymer architectures for a variety of applications, including drug delivery. Given the role of tumor-associated macrophages (TAMs) in cancer and their dependence on the tyrosine kinase receptor FMS (CSF-1R), the key aim of this work was to achieve effective delivery of an FMS inhibitor to cells using a polymer delivery system. Such a system has the potential to exploit biological features specific to macrophages and therefore provide enhanced selectivity. Building on our prior work, we have prepared RAFT polymers based on a P(BMA-*co*-MAA) diblock, which were extended with a hydrophilic block, cross-linker and mannose-based monomer scaffold; exploiting the abundance of macrophage mannose receptors (CD206) on the surface of macrophages. We demonstrate that the prepared polymers can be assembled into nanoparticles and are successfully internalized into macrophages, in part, via the macrophage mannose receptor (CD206). Finally, we showcase the developed nanoparticles in the delivery of an FMS inhibitor to cells, resulting in inhibition of the FMS receptor. As such, this study lays the groundwork for further drug delivery studies aimed at specifically targeting TAMs with molecularly targeted therapeutics.

Introduction

Tumor-associated macrophages (TAMs) have re-emerged as a viable target in cancer therapy.[1,2] Recent evidence suggests that macrophages are involved in normal and diseased tissue remodeling and can contribute to angiogenesis, leukocyte infiltration and immunosuppression.[3] Consequently, an abundance of TAMs is correlated with metastases and poor prognosis in a range of cancers, including breast, prostate, ovarian and non-small cell lung cancers.[4,5]

The growth and activity of tumor-associated macrophages are dependent on interactions between the tyrosine kinase receptor FMS (CSF-1R) and macrophage colony-stimulating factor-1 (CSF-1), with continuous CSF1 exposure and CSF-1R mediated signaling being inextricably linked to the development of several tumor types.[6] Thus, targeting the CSF-1R/CSF-1 axis is an attractive strategy to eliminate or repolarize TAMs to the pro-inflammatory, tumouricidal (M1) phenotype.[7] However, a number of FMS kinase inhibitors suffer from poor bioavailability or have a certain degree of promiscuity, leading to off-target effects.[8] Dasatinib, for example, was developed as a dual inhibitor of the Src and Abl tyrosine kinases but has also been reported as a potent inhibitor of FMS kinase.[9] FMS inhibition can also affect osteoclast production, which is useful in the treatment of bone cancers such as osteosarcoma, but obviously problematic for normal bone growth.[9,10] It is therefore essential to design inhibitors that selectively target FMS kinase within TAMS, specifically within the tumor microenvironment. Taking advantage of both the phagocytic nature of macrophages, as well as the high cell surface expression of the lectin family of carbohydrate-binding proteins, one feasible way to achieve such selectivity is to encapsulate known and novel FMS inhibitors into a glycosylated drug delivery system for specific macrophage delivery.

A range of vehicles have been investigated for use in effective drug delivery to macrophages, including liposomes, mesoporous silica nanoparticles (MSNs), dendrimers and carbon nanotubes (CNTs).[11–16] Despite the success that these carriers have had, there are still limitations with solubilization capacity and concerns over biocompatibility, particularly with respect to MSNs and CNTs. Polymeric materials offer solutions to these problems, by providing higher stability, extended circulation time, favorable biodistribution and highly tunable characteristics.[17] Recent advances in controlled polymerization techniques have enabled chemists to prepare a wide range of nano-objects with macrophage-targeting properties, including micelles,[18,19]

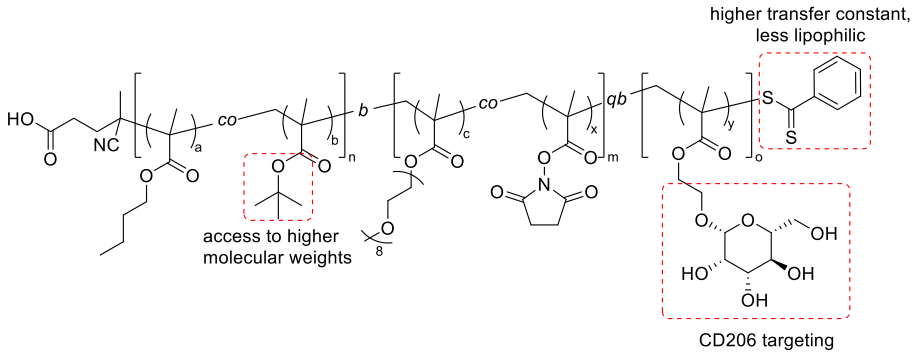

Figure 1. Key design changes to achieve effective delivery to macrophages: CD206-targeting mannose; *t*-Bu-protected methacrylic acid to improve polymerization compatibility and the use of (4-cyano-4-(phenylcarbonothioylthio)pentanoic acid), which has a higher transfer constant and is less lipophilic than the RAFT agent we used previously.

worm-like micelles, [20] polymersomes,[21,22] and polymer-drug conjugates.[23,24] For example, Cui and co-workers recently developed a PEG-sheddable mannosylated nanoparticle to target TAMs *via* mannose-mannose receptor recognition.[25] PEG was used to protect the nanoparticles from rapid elimination and allow for tumor site accumulation. Stenzel and co-workers have also made notable advances in this area with the development of triblock copolymers that were able to self-assemble into several morphologies, ranging from flower-like micelles to so-called 'nanocaterpillars'.[26] These self-assembled materials had an abundance of mannose on the surface and were readily taken up by RAW264.7 macrophages. Glycosylated polymer-drug conjugates have also shown promise; Stayton and co-workers have developed macrophage-targeting drugamers that consist of hydrophilic mannose residues.[27] These residues improve solubility and uptake into alveolar macrophages and lead to a >10-fold increase in sustained ciprofloxacin concentrations inside the cells, whilst increasing overall *in vivo* safety profiles.[27]

Reversible addition-fragmentation chain transfer (RAFT) polymerization is perhaps the most widely used reversible-deactivation radical polymerization (RDRP) method for the synthesis of such polymers; the ease of use, high functional group tolerance and broad versatility in terms of reaction conditions makes this technique highly attractive in the synthesis of block copolymers with low molar mass dispersity.[28, 29] However, there are still drawbacks in terms of scalability, time-consuming purification, and potential for dead chain formation *via* unwanted chain termination. To overcome these limitations, the automated synthesis of quasi-block copolymers *via* sequential RAFT polymerization has recently been reported.[30] We recently reported preliminary studies to use quasi-block copolymers that were able to self-assemble into nanoparticles and deliver a cell-impenetrable dye to macrophages.[31]

In this paper, we have further applied the RAFT methodology to the design and optimization of a glycosylated drug delivery system with macrophage-targeting properties, based on key features from the prior work cited above. The key aim was, for the first time, to achieve effective delivery of an FMS inhibitor to cells. In order to achieve this we modified our initial design[31] by adding a macrophage-targeting sugar moiety and features that would allow for larger polymeric particles, as summarized in **Figure 1**.

Experimental section

Materials. Butyl methacrylate (BMA), poly(ethylene glycol) methyl ether methacrylate (PEGMA-475), 2-hydroxyethyl methacrylate, boron trifluoride diethyl etherate, (3a*R*,5*R*,5a*S*,8a*S*,8b*R*)-2,2,7,7-tetramethyltetrahydro-2*H*,3a*H*,7*H*-bis[1,3]dioxolo[4,5-b:4',5'-*d*]pyran-5-yl]methanol (propylidene acetal-protected galactose) and the RAFT agent used in this work (4-cyano-4-(phenylcarbonothioylthio)pentanoic acid) were purchased from Sigma-Aldrich. *tert*-Butyl methacrylate (tBuMA) was purchased from Tokyo Chemical Industry (UK). Inhibitors were removed from monomers by passing them through an aluminium oxide column prior to use. AIBN was purchased from Sigma-Aldrich and was recrystallized from methanol prior to use. All other reagents were used as received unless otherwise stated. The cross-linker methacrylic acid *N*-hydroxysuccinimide ester was synthesized according to reported literature procedures.[32]

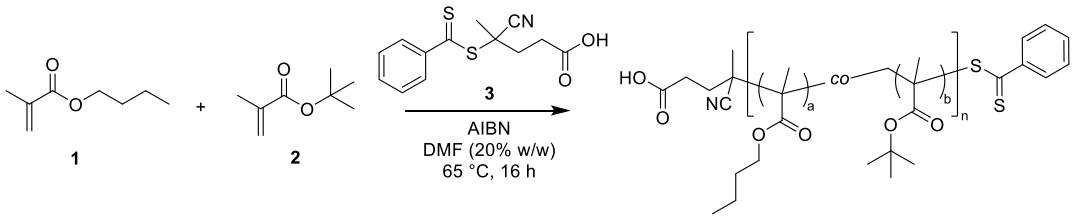

Entry	$[BMA]_0$:$[tBuMA]_0$	[BMA]/[tBuMA] conversions (%)	[BMA]:[tBuMA] (experimental)	Mn (NMR) (kDa)[a]	Mn (SEC) (kDa)[b]	Đ
1	9:1	56.6/68.2	7.5:1	8	8.5	1.14
2	9:1	76.6/100	6.9:1	16	16	1.08
3	9:1	52.8/62.3	7.6:1	24	21	1.11
4	2:1	60.3/71.4	1.7:1	8	13.6	1.17
5	2:1	95.0/73.6	2.6:1	16	14.3	1.18
6	2:1	84.4/66.6	2.5:1	24	27.8	1.57

Table 1. Synthesis of P(BMA-*co*-tBuMA) macro-CTAs. 9:1 feed ratio: $[BMA]_0$:$[tBuMA]_0$:$[CTA]_0$:$[I]_0$ = 188:21:1:0.1; 2:1 feed ratio: $[BMA]_0$:$[tBuMA]_0$:$[CTA]_0$:$[I]_0$ = 28:14:1:0.1 [a]Theoretical number average molecular weight (M_n) was determined by ^{1}H NMR, based on monomer conversion. [b]SEC analyses were obtained by using THF as the mobile phase (calibrated with polystyrene standards).

Synthesis Methods. *1,2,3,4,6-penta-O-acetyl-α-D-mannopyranose (AcMan)*. Sulfuric acid (3 drops) was added, at 0 °C, to a stirred mixture of acetic anhydride (13 mL, 138.5 mmol) and D-mannose (2.5 g, 13.5 mmol) . The reaction mixture was stirred for 1 h at 0 °C, before being warmed to rt and reacted for a further 3 h. The reaction mixture was poured into ice cold water (50 mL) and extracted with dichloromethane. The extract was washed with water (3 x 50 mL), sat. aqueous $NaHCO_3$ (3 x 50 mL), dried ($MgSO_4$) and concentrated *in vacuo* to afford a colorless oil. Excess acetic anhydride was then removed azeotropically with toluene, affording the title compound as a thick, colorless oil (5.13 g, 97%). ^{1}H NMR (400 MHz, Chloroform-*d*) δ 6.07 (d, *J* = 1.9 Hz, 1H), 5.36 – 5.31 (m, 2H), 5.27 – 5.23 (m, 1H), 4.32 – 4.24 (m, 1H), 4.12 – 3.99 (m, 2H), 2.16 (s, 3H), 2.16 (s, 3H), 2.08 (s, 3H), 2.04 (s, 3H), 1.99 (s, 3H). ^{13}C NMR (101 MHz, Chloroform-*d*) δ 170.6, 170.0, 169.7, 169.5, 168.0, 90.6, 90.4, 73.3, 70.6, 68.7, 68.3, 65.6, 62.1, 20.8, 20.7, 20.7. MS (ES+) *m*/*z* 391 $[M+H]^+$.

2-[(2,3,4,6-tetra-O-acetyl-α-D-mannopyranosyl)oxy]ethyl 2-methylprop-2-enoate (AcManMA). AcMan (2.5 g, 6.4 mmol) and 2-hydroxyethyl methacrylate (0.83 g, 7.4 mmol) were dissolved in anhydrous dichloromethane (30 mL) under N_2 flow. Boron trifluoride diethyl etherate (4.54 g, 32 mmol) was added dropwise over a 10-15 min period with a gastight syringe and the solution was purged with N_2 for 20 min. The flask was stirred at rt for 72 h to allow for full conversion. The reaction mixture was concentrated *in vacuo*, dissolved in ethyl acetate (100 mL) and poured into ice cold water. The aqueous layer was then extracted with ethyl acetate (3 x 50 mL) and the combined organic layer was washed with sat. aqueous $NaHCO_3$ (3 x 100 mL), brine (3 x 100 mL) and water (3 x 100 mL). The organic layer was dried ($MgSO_4$) and concentrated *in vacuo* and the resultant crude oil was then purified via column chromatography (10% EtOAc/DCM), affording the title compound as a white solid (1.39 g, 49%). ^{1}H NMR (400 MHz, Chloroform-*d*) δ 6.15 – 6.10 (m, 1H), 5.60 (t, *J* = 1.6 Hz, 1H), 5.38 – 5.22 (m, 3H), 4.87 (d, *J* = 1.8 Hz, 1H), 4.37 – 4.31 (m, 2H), 4.27 (dd, *J* = 12.2, 5.5 Hz, 1H), 4.10 – 3.99 (m, 2H), 3.95 – 3.70 (m, 2H), 2.15 (s, 3H), 2.09 (s, 3H), 2.04 (s, 3H), 2.03 (s, 3H), 1.99 (s, 3H), 1.95 (t, *J* = 1.3 Hz, 3H). ^{13}C NMR (101 MHz, Chloroform-*d*) δ 170.7, 170.1, 169.9, 169.7, 167.1, 136.0, 126.1, 97.5, 69.4, 69.0, 68.6, 66.1, 65.9, 63.2, 62.4, 21.1, 20.9, 20.8, 20.7, 18.3. HRMS TOF MS ES+ (*m*/*z*): $[M+Na]^+$ calc'd for $C_{19}H_{26}O_{12}Na$: 483.1489; found: 483.1486.

[(3aR,5aS,8aS,8bR)-2,2,7,7-tetramethyltetrahydro-2H,3aH,7H-bis[1,3]dioxolo[4,5-b:4',5'-d]pyran-5-yl]methyl 2-methylprop-2-enoate (GalMA). To a stirred solution of (3a*R*,5*R*,5a*S*,8a*S*,8b*R*)-2,2,7,7-tetramethyltetrahydro-2*H*,3a*H*,7*H*-bis[1,3]dioxolo[4,5-b:4',5'-*d*]pyran-5-yl]methanol (5 g, 19.2 mmol), and basic aluminium oxide (3.9 g, 88.2 mmol) in anhydrous acetonitrile (50 mL), methacryloyl chloride (10.3 g, 98.9 mmol) was added at rt and was left to stir for 4 d. The reaction was monitored by TLC and when a suitable level of conversion was reached, the reaction mixture was concentrated *in vacuo*. The crude mixture was then purified by column

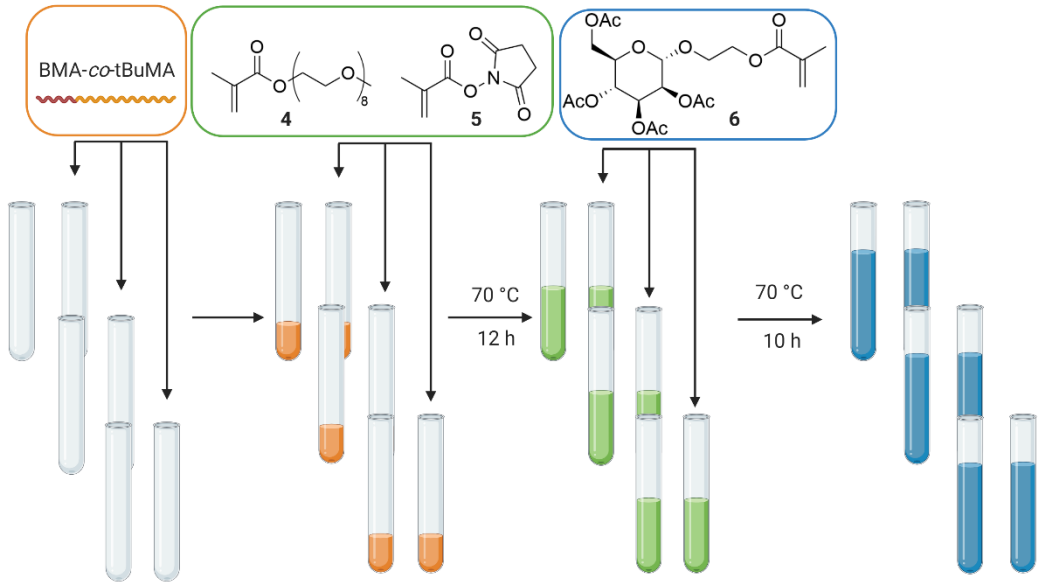

Reactor no.	Macro-CTA (entry from Table 1)	[NMS]:[PEGMA]:[AcManMA]*	NMR[a]	SEC[b]		D_H (DLS)	
			M_n (kDa)	M_n (kDa)	$Đ$	(nm)	PDI
1	**1**	7:1:11	24.0	13.3	1.18	127	0.22
2	**1**	11:4:9	25.1	14.1	1.16	131	0.30
3	**2**	5:2:15	32.1	23.8	1.21	295	0.31
4	**2**	10:3:9	31.0	26.7	1.12	268	0.27
5	**3**	5:2:8	37.5	35.5	1.14	135	0.22
6	**3**	9:3:8	39.0	31.0	1.21	200	0.26
7	**4**	3:2:9	42.3	46.8	1.08	329	0.26
8	**4**	8:3:9	44.0	46.5	1.06	195	0.08
9	**5**	5:2:11	32.7	34.5	1.05	81	0.23
10	**5**	9:3:8	32.7	34.7	1.04	88	0.27
11	**6**	6:2:11	38.3	34.8	1.04	109	0.27
12	**6**	9:2:9	36.7	33.0	1.05	100	0.24

Table 2. Automated synthesis of quasi-block copolymers. $[\text{macro-CTA}]_0:[I]_0$ = 1:0.1. *Experimentally determined ratios. [a]Theoretical number average molecular weight (M_n) was determined by ^{1}H NMR, based on monomer conversion. [b]SEC analyses were obtained by using THF as the mobile phase (calibrated with polystyrene standards). The hydrodynamic volume of the deprotected polymers was measured with DLS and based on the intensity mean.

chromatography (3% EtOAc:DCM, rf = 0.3), affording the title compound as a white solid (5.58 g, 88%). ^{1}H NMR (400 MHz, Chloroform-*d*) δ 6.02 (s, 1H), 5.46 (s, 1H), 5.42 (d, J = 4.9 Hz, 1H), 4.52 (dd, J = 7.9, 2.5 Hz, 1H), 4.27 – 4.19 (m, 2H), 4.18 – 4.08 (m, 2H), 4.02 – 3.91 (m, 1H), 1.83 (s, 3H), 1.39 (s, 3H), 1.34 (s, 3H), 1.23 (s, 3H), 1.22 (s, 3H). ^{13}C NMR (101 MHz, Chloroform-*d*) δ 167.0, 136.0, 125.6, 109.5, 108.6, 96.2, 71.0, 70.6, 70.4, 66.0, 63.6, 25.8, 24.9, 24.3, 18.2. HRMS TOF MS ES+ (*m/z*): $[M+MeCN+H+Na]^+$ calc'd for C18H27NO7Na: 392.1685; found: 392.1675.

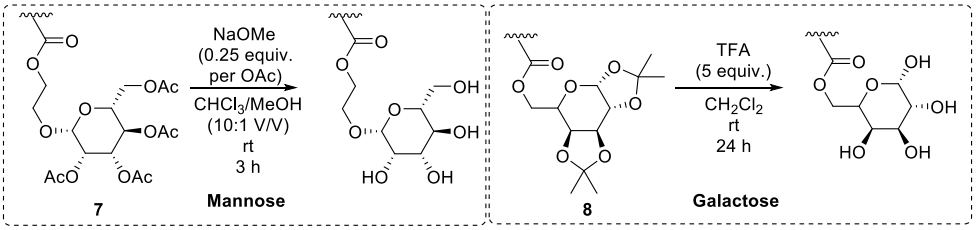

Figure 2. Deprotection conditions for mannose-based copolymer P(BMA-*co*-tBuMA-*b*-NMS-*co*-PEGMA-*qb*-AcManMA) and galactose-based copolymer P(BMA-*co*-MAA-*qb*-NMS-*qb*-PEGMA-*co*-GalMA).

Polymer Synthesis. *P(BMA-co-tBuMA) macro-CTA (example)*. With a target MW of 30 kDa and DP[BMA] = 188, DP[*t*BuMA] = 21: *tert*-butyl methacrylate (594 mg, 4.18 mmol), butyl methacrylate (5.34 g, 37.6 mmol), 4-cyano-4-(phenylcarbonothioylthio)pentanoic acid (55 mg, 0.2 mmol) and AIBN (6.5 mg, 40 μmol) were dissolved in DMF (26 mL) along with 1,3,5-trioxane (~10 mg) as an internal standard. The reaction mixture was degassed by sparging with N_2 for 30 min, before being heated to 70 °C for 16 h. Conversion was monitored by ^{1}H NMR (<80%) and the reaction mixture was cooled to rt. The polymer solution was then dialyzed against water for 48 h, followed by lyophilization, affording the polymer as a pink solid (3.62 g, 60%).

Automated Synthesis of Quasi-Block Copolymers. The commercially available synthesizer utilized in this work was a Chemspeed Swing-SLT automated parallel synthesizer. The synthesizer was equipped with a glass reactor block consisting of 16 reaction vessels (13 mL) with thermal jackets connected in series through the reaction block and connected to a heating/cooling system (Huber, -90 °C to 140 °C). In addition, all reaction vessels were equipped with cold-finger reflux condensers (~7 C). Mixing was achieved by vortex agitation (up to 1400 rpm). Liquid transfers were handled by a 4-needle head (4-NH) capable of four simultaneous sample transfers. The 4-NH was connected to a reservoir bottle (degassed DMF solvent) for needle rinsing after each liquid transfer step. This DMF solvent reservoir was degassed by continuous sparging with nitrogen and was also utilized to prime the tubing lines of the 4-NH. When experiments were carried out, the synthesizer was maintained under an inert atmosphere by supplying a constant flow of nitrogen into the hood of the synthesizer. A nitrogen atmosphere was also applied to reactors and stock solutions at all times. Prior to the experiments, the reaction vessels were heated to 135 °C and subjected to 10 cycles of vacuum (2 min each) and filling with nitrogen (2 min each) to ensure the elimination of oxygen. After this pre-treatment, the RAFT polymerization experiments were carried out following similar procedures as reported above(although utilizing an automated parallel freeze–evacuate–thaw degassing method rather than N_2 sparging).

Deprotection Conditions. *Mannose Deprotection.* P(BMA-*co*-MAA-*qb*-NMS-*co*-PEGMA-*qb*-AcManMA) (190 mg, 0.025 mmol – assuming 7.5 kDa polymer) was dissolved in a chloroform/methanol (28 mL: 2 mL) mixture and degassed with N_2 at 0 °C for at least 40 min. Sodium methoxide (5.4 mg of a 25% solution, 0.025 mmol, 0.25 equiv. per acetyl group) was then added and the reaction mixture was stirred for 3 h at rt, generating a cloudy mixture. The resultant solution was then purified by dialysis against water for 48 h, with a minimum of two changes of water. The purified polymer was then lyophilized to yield the title polymer as a white solid (108 mg, 59%).

tert-Butyl Deprotection. General procedure for deprotection: the polymer was dissolved in dichloromethane, followed by the addition of trifluoroacetic acid (5 equivalents, 1 per *t*-Bu group). The reaction mixture was then left to stir at rt for 24 h. Successful deprotection was confirmed by ^{1}H NMR. Upon completion of the reaction, the polymer was purified by dialysis against water for 48 h, with a minimum of two changes of water. Any resultant polymer was then dried in a vacuum oven at 30 °C, unless otherwise indicated.

Galactose Deprotection. P(BMA-*co*-MAA-*b*-NMS-*co*-PEGMA-*qb*-GalMA) (20 mg, 1 μmol) was dissolved in formic acid (98-100% solution, 1 mL) and was stirred at 60 °C for 1 h. The solution was then cooled to rt and purified by dialysis against water for 48 h, with a minimum of two changes of water. The purified polymer was then lyophilized to yield the title polymer as a white solid (13 mg). Loss of isopropylidene signal at 1.53 ppm (^{1}H NMR) confirmed successful deprotection.

Polymer Characterization. *^{1}H NMR.* All spectra were recorded on a Bruker Advance 400 MHz spectrometer and were analyzed with MestReNova software. Monomer conversion was measured by analysis of the reduction in the olefinic peaks against an internal standard (1,3,5-trioxane). Exact DP of the macro-CTA chain extensions were calculated from the initial macro-CTA NMRs.

Gel Permeation Chromatography (GPC). Gel permeation chromatography (GPC) was performed on a Waters Alliance system equipped with an Alliance 2695 Separations Module (integrated quaternary solvent delivery, solvent degasser and autosampler system), a Waters column heater module, a Waters 2414 RDI refractive index detector, a Waters PDA 2996 photodiode array detector (210 to 400 nm at 1.2 nm) and 4 × Agilent PL-Gel columns (3 x PL-Gel Mixed C (5 μm) and 1 x PL-Gel Mixed E (3 μm) columns), each 300 mm × 7.8 mm^2, providing an effective molar mass range of 200 to 2 × 10^6). Tetrahydrofuran (THF) high purity solvent (HPLC grade) was pre-filtered through aluminium oxide (90 active neutral, 70-230 mesh) with 0.45 μm filter, and 0.1 gL^{-1} 2,6-di-*tert*-butyl-4-methylphenol (BHT) was added as inhibitor. The filtered THF containing BHT was purged slowly with nitrogen gas and used as an eluent with a flow rate of 1 ml min-1 at 30 °C. Number (M_n) and weight average (M_w) molar masses were evaluated using Waters Empower-3 software. The GPC columns were calibrated with low dispersity polystyrene standards (Polymer Laboratories)

ranging from 580 to 7,500,000 g mol^{-1} and molar masses are reported as polystyrene equivalents. A 3rd-order polynomial was used to fit the log Mp vs. time calibration curve, which was near linear across the molar mass ranges.

Dynamic Light Scattering. Measurements were performed on a Beckman Coulter DelsaNano C Particle Analyzer. BRAND Macro Polystyrene (PS) Cuvettes were used.

Cross-linking and drug loading. Cross-linking was achieved by adding JEFFAMINE-D230 directly to the aqueous polymer solution post-deprotection, followed by stirring for 24 h. Further dialysis for 48 h, followed by lyophilization, afforded the cross-linked polymer. For drug loading, the cross-linked material was co-dissolved in DMF (1 mL) at a concentration of 20 mg/mL with the drug to be loaded onto the core (2 mg/mL). Water (5 mL) was then added dropwise with rapid stirring. The drug-loaded, cross-linked micelles were then dialyzed for 24 h, followed by lyophilization. Drug loading was then assessed with UV-vis spectroscopy (dasatinib λ_{max} = 323 nm).

The drug loading efficiency (DLE) was determined according to the following equation:

$$\text{DLE} = \frac{\text{mass of drug loaded onto micelles}}{\text{mass of drug initially added}} \text{ x } 100$$

***In Vitro* Uptake Studies.** *Mice.* C57Bl/6 mice were bred at Monash Animal Research Platform (Monash University, Clayton, Australia). Both male and female mice were used and were 6–12 weeks of age.

Cell Isolation. The outer skin was removed from the area surrounding the peritoneal cavity and PBS-2% FBS (10 ml) was slowly injected into the cavity through a 16-gauge needle. The area was gently massaged to dislodge and resuspend cells before the cell suspension was aspirated by syringe needle. Approximately 2 x 10^6 cells were obtained per mouse.

Flow Cytometric Analysis. Cells were immunolabelled for flow cytometry with an antibody cocktail containing any of the following (specified for each experiment): F4/80-AF647, F4/80-BUV395, CD11b-AF647, CD11b-FITC, CD206(MMR)-PECy7. TruStain fcX anti-mouse CD16/32 was used for blocking.(note: CD11b is also referred to as Mac-1). Flow cytometric analysis was performed on an LSR II (BD Biosciences) with 7 solid state lasers: 355 nm 405 nm, 488 nm, 532 nm, 561 nm, 592 nm and 628 nm. Flowjo X was used to analyze all flow cytometry data. The internalization of particles was determined by rhodamine fluorescence detected in cells. Rhodamine was excited with the 561 nm laser and fluorescence emission was detected with a 564–606 nm band pass filter.

Mannose Pre-treatment Studies. Murine peritoneal macrophages (1 x 10^6/mL) were incubated with a solution of D-mannose (100 µL, 50 mM) in PBS at 37 °C for 30 min. Cells with no mannose treatment were used as controls. After incubation, the cells were thoroughly washed with PBS and were resuspended in polymer solution (100 µL, 10 µg/mL) at 0 °C for 30 min. The cells were then warmed to rt for 5 min, washed and then immunolabelled with anti-F4/80 and anti-CD11b antibodies for 15 min at 0 °C. The cells were washed, resuspended in PBS (2% FBS) containing propidium iodide (PI; 0.1 µg/mL) and analyzed by flow cytometry.

Anti CD206 Studies. Primary peritoneal macrophages (1 x 10^6/mL) were treated with polymer solutions (100 µL, 10 µg/mL) at 0 °C for 30 min. The cells were warmed to rt for 5 min, thoroughly washed with PBS and were blocked with TruStain fcX anti-mouse CD16/32 (50 µL) at 0 °C for 10 min. The cells were washed with PBS and then treated with anti-CD206, F4/80 and CD11b antibodies for 15 min at 0 °C. The cells were washed, resuspended in PBS (2% FBS) containing propidium iodide (PI; 0.1 µg/mL) and analyzed by flow cytometry.

Transformation Assay with Rat-2 fibroblasts. For transformation assays, Rat-2 fibroblasts had previously been stably infected using a retrovirus containing V-fms (Rat-2 v-fms) or c-fms (Rat-2 c-fms) as described previously.[9] These cells were seeded at 1 x 10^4 cells/ml in Dulbecco's Modified Eagles Media (Invitrogen, Paisley, UK) + 10 % FCS, cultured for 24 h. These were then treated with dasatinib-loaded nanoparticles and incubated for a further 2 h, followed by Western blot analysis.

Results and Discussion

Synthesis of hydrophobic macro-CTA

Initial polymer designs were based on a P(BMA-*co*-MAA) diblock copolymer scaffold that had been previously synthesized by our group, due to its efficient dye-loading and cellular uptake properties.[31] Butyl methacrylate (BMA, **1**, **Table 1**) and *tert*-butyl methacrylate (tBuMA, **2**) were copolymerized at 65 °C in DMF in the presence of dithiobenzoate-based RAFT agent, 4-cyano-4-(phenylcarbonothioylthio)pentanoic acid (CPT, **3**), with AIBN as the radical initiator. A full synthetic route for these materials can be found in the supporting information (**Scheme S1**). CPT was chosen as the RAFT agent due to its high transfer constant and less hydrophobic R group (relative to the trithiocarbonate-ACVA hybrid RAFT agent, 4-cyano-4-[(dodecylsulfanylthiocarbonyl)sulfanyl]pentanoic acid), which may have impacted on the stability of the nanoparticles formed in our previous work.[31] The major challenge in accessing high MW polymers with our original system, particularly the hydrophobic block, was the incompatibility in the kinetics of methacrylic acid (MAA) and butyl methacrylate (BMA). This incompatibility becomes much more pronounced when targeting higher molecular weights because a higher proportion of dead chains are produced (non-polymerizable chains that result from bimolecular termination and side reactions), which in turn raises the molar mass dispersity.

Rizzardo and co-workers first reported the polymerization of acid-based monomers using RAFT polymerization.[33] They polymerized acrylic acid (AA) and found that the process was extremely slow compared to other monomers (18% conversion after 4 h at 60 °C).[33] There have, however, been a number of developments since these early polymerizations. P(AA)-based copolymers can now be made *via* RAFT polymerization under a range of optimized conditions.[34–36] Much of these involve aqueous solvents or emulsion polymerization processes and would remain incompatible with polymerization directly with BMA in the same block.

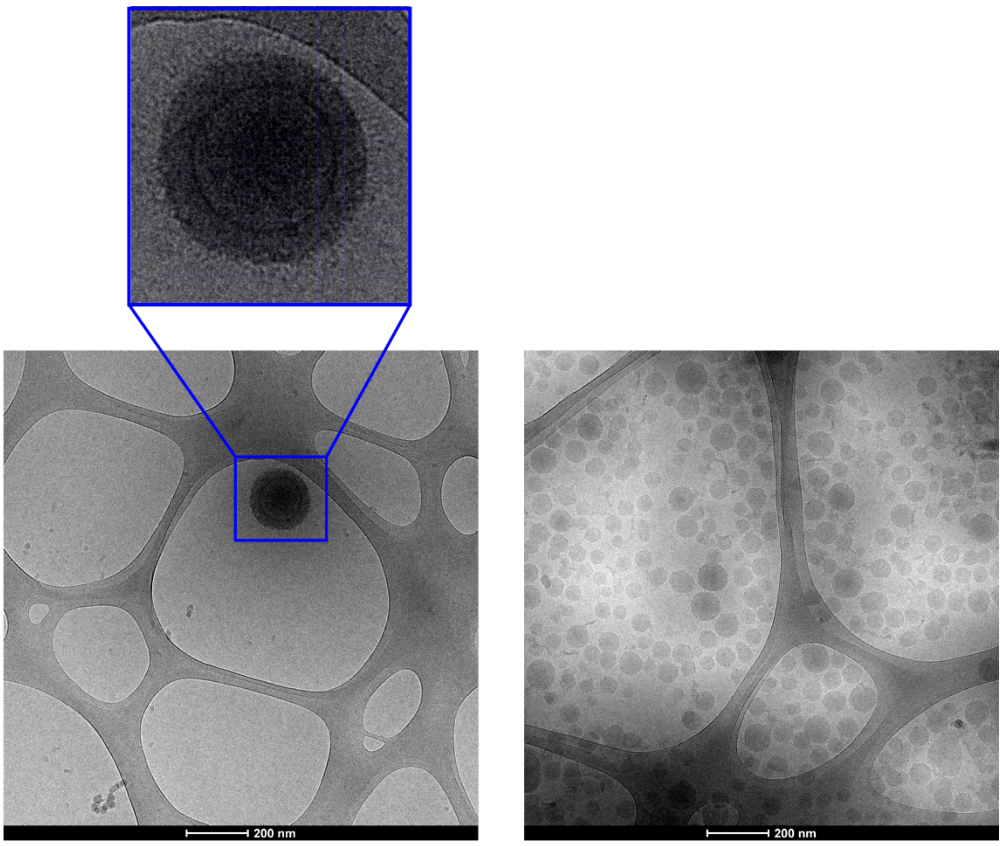

Figure 3. Cryo-TEM images of protected and deprotected copolymer compositions after large scale batch synthesis based on results from the ChemSpeed. Left (1): P(BMA-*co*-tBuMA-*b*-NMS-*co*-PEGMA-*qb*-AcManMA). A clear bilayer can be seen in these structures; right (2): P(BMA-*co*-MAA-*b*-NMS(Jeff)-*co*-PEGMA-*qb*-ManMA). Deprotection and cross-linking with NMS led to the formation of a less uniform population of nanoparticles. Scale bar: 200 nm.

To overcome these incompatibility issues, the *tert*-butyl ester of methacrylic acid was chosen; tBuMA and BMA have a very similar kinetic profile, which allows for the formation of copolymers with well-defined MWs and narrow molar mass dispersities.

The results of these preliminary polymerizations are summarized in **Table 1.** These macro-chain transfer agents (macro-CTAs) were made with very narrow monodispersities (M_w/M_n <1.20) and the reactions were stopped at <80% conversion to ensure high end-group fidelity. The high levels of control over the polymerization process is consistent with our previous work (M_w/M_n ranged from 1.16 to 1.42), thereby highlighting the versatility of RAFT in the synthesis of vehicles for drug delivery.[31] The comonomer molar contents in the copolymers were estimated from ^{1}H NMR analysis against an internal standard (1,3,5-trioxane) and verified by gel permeation chromatography (see **SI Section 2.8**). Following synthesis, the macro-CTAs were purified *via* dialysis against water to afford pure copolymers. These were chain extended to afford copolymers with both pure- and quasi-block characteristics.

Chain extension of macro-CTA *via* automated synthesis

Following successful synthesis of the hydrophobic core, the resultant copolymer was used as a macromolecular chain transfer agent (macro-CTA) to generate quasi-block copolymers *via* sequential polymerization. The copolymerizations were carried out on an automated platform with robotic handling of the reaction components. The resultant polymers are summarized in **Table 2.** The hydrophilic chain, consisting of PEGMA-495 **4**, the cross-linker methacrylic acid *N*-hydroxysuccinimide ester (NMS, **5**) and acetylated mannose-based monomer (AcManMA, **6**) were then added in varying molar ratios, affording polymer chains in a variety of MWs. These target MWs and molar ratios were chosen to explore the impact that polymer composition, particularly high loading of the hydrophobic

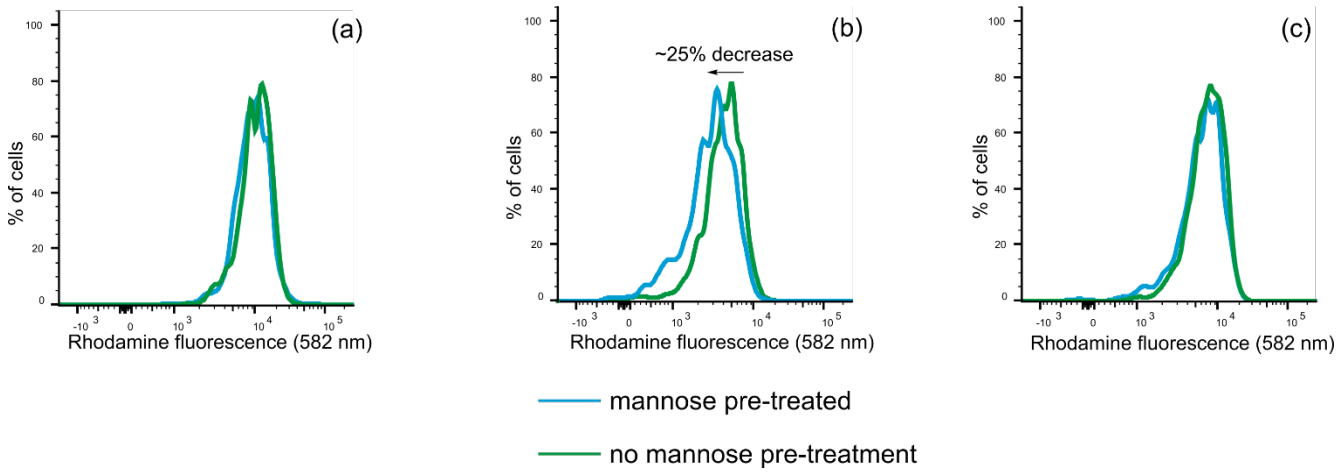

Figure 4. Assessment of rhodamine fluorescence in primary murine macrophages ($Mac1^+F4/80^+$) that were treated with glycosylated copolymers (10 μg/mL) at 0 °C (to promote receptor binding) followed by brief incubation at rt (to promote internerlization). (a) = P(BMA-*co*-MAA-*qb*-NMS-*qb*-PEGMA-*co*-GalMA); (b) = P(BMA-*co*-MAA-*qb*-NMS-*qb*-PEGMA-*co*-ManMA); (c) = P(BMA-*co*-MAA-*qb*-NMS-*qb*-PEGMA). A difference in uptake is observed with the mannosylated copolymers between the cells that have been pre-treated with mannose vs. the non-pre-treated population. No CD206 gating was carried out on these cells. Polymers used were from batch synthesis post-ChemSpeed: Mannose-based copolymer: P(BMA-*co*-MAA-*qb*-NMS-*qb*-PEGMA-*co*-ManMA - (M_n = 14.5 kDa, $Đ$ = 1.55)); galactose-based copolymer: P(BMA-*co*-MAA-*qb*-NMS-*qb*-PEGMA-*co*-GalMA)(M_n = 13.5 kDa, $Đ$ = 1.54); no sugar: P(BMA-*co*-MAA-*qb*-NMS-*qb*-PEGMA).

portion, had on the size and morphology of the resultant nanoparticles.

NMS was incorporated as a reactive monomer and self-assembled nanoparticles were crosslinked with the diamine crosslinker, JEFFAMINE-D230, a polyetheramine commonly used to cross-link hydrogels in order to provide mechanical stability.[37] This reactive monomer was used in our previous nanoparticle design to provide additional stability in a range of different media and to retain nanoparticle integrity below the critical micelle concentration (CMC). While it is likely that partial hydrolysis of the NHS ester may have occurred during the deacetylation reaction, successful crosslinking of these nanoparticles was confirmed by assessing their stability in a range of organic solvents by DLS (**Table S1**).[31] In the presence of JEFFAMINE-D230, polymers formed stable nanoparticles in both isopropanol and THF, but were unstable in its absence. This confirms the success of the cross-linking chemistry.

Mannose was incorporated to take advantage of the abundance of macrophage mannose receptors (CD206) on the surface of macrophages.[38,39] Galactose-based copolymers were also synthesized as a control for biological uptake studies; mannose should have a higher affinity for our receptor of interest, CD206, than galactose and therefore uptake should be higher with mannose-based copolymers.[40] The interaction between single carbohydrate molecules and lectins (carbohydrate binding proteins) on the surface of cells is highly specific, but usually very weak (association constants $>10^6$ M^{-1}).[41] However, multivalent interactions, from a polysaccharide chain for example, can increase the strength of the binding by many fold.[42] This phenomenon is known as the cluster glycoside effect, and was first coined by Lee and co-workers.[43] Both acetyl-protected mannose- and propylidene acetal-protected galactose- monomers were polymerized. These polymerizations were carried out in their protected form to prevent solubility issues and allow for the RAFT process to proceed smoothly.[26,44] It is notable that RAFT polymerization allows the polymerization of glycosylated materials directly, without the need for post-polymerization functionalization, due to its wide functional group tolerance.

The experimental (GPC) M_n for entries 4 to 12 are in good agreement with the theoretical calculations (^{1}H NMR – see **SI Section 2.5**) and the molar mass dispersity ($Đ$) is low, which is indicative of good control over the polymerization process. Many chain extensions in **Table 2** led to a reduction in $Đ$, which may have resulted from partial collapse of the polymer chain due to the pendant PEG moieties. This can result in decreased hydrodynamic volumes by SEC, thereby resulting in a decrease in both M_n and $Đ$.[45–47] The deviation in entries 1 to 4 can be attributed to the difference between the hydrodynamic volumes of the polystyrene standards used in the GPC measurements and the methacrylate backbone.[30]

The polymers were then deprotected in either one (galactose) or two (mannose) steps (**Figure 2**). For mannose-based copolymers **7**, the pendant mannose moieties were deacetylated under basic conditions, following a procedure reported by Stenzel and co-workers.[26] The copolymer was dissolved in an anhydrous $CHCl_3$/MeOH mixture and treated with sodium methoxide (0.25 equivalents per acetate group), followed by dialysis and lyophilization. The reaction was monitored by qualitatively assessing the disappearance of the acetyl peaks at 2.0-2.4 ppm

(^{1}H NMR). Deprotection was confirmed *via* a combination of ^{1}H NMR, GPC and DLS. This protocol was then applied to all future deprotections. It should be noted that by ^{1}H NMR, any hydrolysis of the polymer backbone esters appeared to be minimal. Zemplén deprotection is commonly used in the deprotection of glycopolymers with minimal degradation.[48–53] However, an in-depth study to examine the affect that this reaction can have on other polymeric esters would be of great interest.

The control polymer, galactose-based copolymer **8**, was deprotected under acidic conditions. Formic acid was initially chosen to avoid unwanted degradation of the polymer backbone when TFA was used – a problem that had previously been reported by Stenzel and co-workers.[54] We later found, however, that the TFA deprotection methodology used to deprotect the *t*-Bu ester also simultaneously removed the acetal groups, affording the desired polymer in one step. Minimal degradation of the rest of the polymer was observed by ^{1}H NMR.

The *tert*-butyl groups were then removed from the copolymers under acidic conditions, following a procedure developed by Colombani and co-workers. [55] The copolymer was treated with five equivalents of trifluoroacetic acid (TFA – relative to *tert*-butyl groups) at room temperature for 48 hours. Following successful removal of the *tert*-butyl groups (confirmed by ^{1}H NMR), the reaction mixture was concentrated and dissolved in MeOH, followed by dialysis against water for 48 hours. ^{19}F NMR was then conducted to determine the presence of residual TFA. If any TFA remained, the copolymer was dissolved in MeOH and passed through a PD-10 desalting column.

The hydrodynamic radii of the self-assembled nanoparticles were assessed using DLS and sizes ranged from 81 nm to 329 nm, which is indicative of the formation of micellar aggregates and higher order structures. AcManMA and PEGMA were not evenly incorporated across the 12 polymers given the quasi-block approach, therefore direct comparisons cannot be made between the molar ratios. However, there is an interesting trend between the M_n and hydrodynamic diameter (D_H), as shown in the SI (**Figure S24**); there is a clear increase in the formation of aggregate and higher order structures (D_H=200-300 nm) between 14 and 31 kDa, as the loading of the hydrophobic component was large relative to the hydrophilic component. The D_H then decreased to ~100 nm between 33 and 40 kDa, which is more indicative of true micelles. Aggregation effects then begin to re-occur at 40 kDa and above.

Upon further examination with transmission electron cryomicroscopy (cryo-TEM) (**Figure 3**), it was found that the protected copolymers displayed high levels of aggregation, presumably due to the hydrophobic acetyl protecting groups present on the mannose monomers. As these protecting groups were in the hydrophilic block, efficient self-assembly was more challenging and it is likely that the polymer chains folded in on themselves, exposing the pendant PEG. However, it was clear that spherical micelles were still formed to a degree, as well as larger self-assembly constructs such as polymersomes.

A central bilayer is clearly visible on acetyl-protected copolymer P(BMA-*co*-MAA-*b*-NMS-*co*-PEGMA-*qb*-AcManMA). The TEM image of mannose deprotected copolymer P(BMA-*co*-MAA-*b*-NMS(Jeff)-*co*-PEGMA-*qb*-ManMA) is also consistent with the DLS results; this is a mannose-containing copolymer that has been fully deprotected (exposing both methacrylic acid and sugar moieties) and cross-linked with JEFFAMINE-D230. This polymer appears to form populations of uniform micelles of 50 and 80 nm in diameter. The homogeneity of these morphologies can be controlled by the rate of addition of water to the DMF solution of copolymer.

The goal for this screen was to identify a polymer composition that can generate larger nanoparticles and higher order structures such as polymersomes, in order to take advantage of the phagocytic nature of macrophages. **Entries 2**, **3** and **4** were particularly promising as these self-assembled into micellar-type structures above the traditional size for micelles (>100 nm) but were less prone to aggregation effects compared to the polymers >35 kDa. We also found that polymers between 10 and 20 kDa with a relatively high sugar loading relative to PEGMA (3:1) were also able to generate larger polymersome-like morphologies. These were characterized with a combination of DLS and cryo-TEM. Given that polymeric materials with molecular weights <20 kDa have been shown to penetrate deeper into solid tumors [56] and materials >30 kDa begin to reach the renal clearance threshold,[57] we ultimately selected a composition that balanced particle size, sugar loading and efficient drug loading/release for characterization in preliminary biological assays.

Batch synthesis of selected polymers and drug loading

Based on the synthetic work carried out with the automated synthesizer, 20 kDa triblock copolymers were synthesized on a larger scale. Galactose-functionalized materials were also made as a control for biological uptake studies. These materials were then labelled with fluorescent monomer, rhodamine B isothiocyanate (RhoB) for use in biological uptake assays. An overall MW of 13 to 16 kDa and M_w/M_n of approximately 1.5 was obtained for each material post-deprotection. Following the cross-linking step, DLS analysis indicated a particle size of around 100 nm, which is in close agreement with the trends observed in **Table 2**. The size and polymersome-like morphology of the glycopolymers was confirmed by cryo-TEM.

Drug loading of the particles was then investigated. The strategy used relied on the hydrophobicity of the particle core to stabilize the drug-particle interaction, which is further stabilized by outer-corona/shell cross-linking. This is a direct development from our previous work, which demonstrated the delivery of a cell-impenetrable dye as a proof of concept. [31] The tyrosine kinase inhibitor dasatinib was chosen as a model substrate as it has been shown to be a potent inhibitor of TAMs and FMS kinase.[9] Furthermore, the slightly basic nature of this drug should further stabilize the drug-particle *via* acid-base interactions with the methacrylic acid monomer unit.

Drug loading was achieved by dropwise addition of water to a 20 mg solution of polymer, co-dissolved with 2 mg of dasatinib in 1 mL of DMF. The resultant suspension was then dialyzed against water for 48 hours, followed by lyophilization. The polymer-drug nanoparticles were then resuspended in water and UV-vis spectroscopy was used to determine the concentration of dasatinib in the core against a previously determined concentration curve at the dasatinib λ_{max} of 323 nm. Polymers with a 2:1 ratio of BMA:MAA showed at least a two-fold increase in drug loading efficiencies (10% DLE) compared to a 9:1 ratio (5% DLE). However, higher molar ratios of BMA in the core led to polymers with the desired self-assembly characteristics (*vide supra*) and still allowed for loading of µM concentrations of dasatinib. Therefore the 9:1 ratio of BMA:MAA was maintained for biological studies.

A leakage study was also carried out with UV-Vis spectroscopy to determine the rate of drug release in solution and therefore stability of the nanoparticle encapsulated cargo prior to cell treatment (**SI, Figure S29**). Within the first hour, only ~1.5% of the total drug loaded had been released into solution. Following this initial period however, the rate of leakage slowed dramatically to approximately 0.2%/h, which suggests that these nanoparticles are stable in solution. Nevertheless, nanoparticle solutions were prepared fresh for each experiment in biological studies.

To determine the stability of the nanoparticles in media containing serum, lyophilized dasatinib-containing P(BMA-*co*-MAA-*b*-NMS(Jeff)-*co*-PEGMA-*qb*-ManMA) polymer nanoparticles were resuspended in either PBS or 55% v/v human serum in PBS. A 55% dilution of serum was chosen as this mimics the concentration of *in vivo* serum proteins.[58] These nanoparticle suspensions were then dialyzed against PBS at 37 °C for 24 h. At 6 h and 24 h, the dialysis membranes were opened, and aliquots were taken for analysis by UV-Vis spectroscopy (**SI, Figure S30**). Drug release was determined by comparing the absorption of dasatinib (λ_{max} of 323 nm) at each given time point, relative to the concentration at t = 0 h. After 6 h, 4.5% of dasatinib had been released in PBS, and 17.5% had been released in the solution containing human serum. After 24 h, 31.3% and 35.7% had been released in PBS and the solution containing human serum, respectively.

In addition to examining the stability of the drug-nanoparticle interaction, the integrity of the nanoparticles after 24 h incubation in human serum was assessed with DLS (**SI, Figure S31**). Both PBS and serum-incubated nanoparticle suspensions gave similar results, with a Z-average of 225 nm and 250 nm, respectively. Larger aggregate structures were observed in samples incubated in serum; however, this was attributed to the large serum proteins. Filtration of the suspension (0.45 µm filter) to remove the proteins afforded nanoparticles that were consistent in size with the PBS control, indicating that these nanoparticles remain stable in the presence of serum proteins.[59]

Assessment of uptake in primary macrophages

In our previous work we examined the uptake of a series of cross-linked copolymers into primary macrophages and showed the particles to be efficiently internalized.[31] Given that our new designs now contain sugar units, we were interested in the role of glycosylation for uptake. Mannose receptors play a central role in innate and immune responses. The macrophage mannose receptor (MMR; CD206) is a transmembrane protein that binds

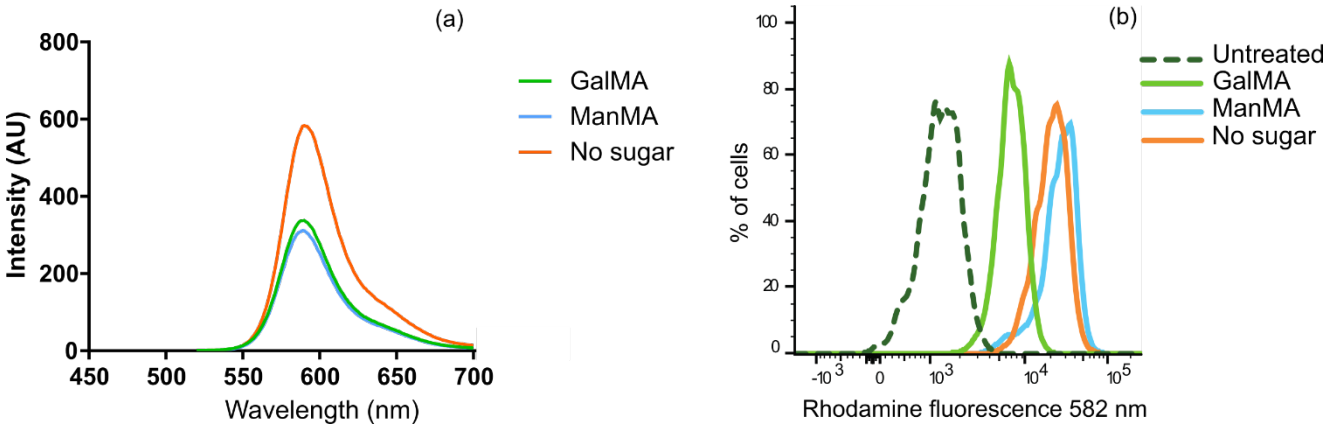

Figure 5 (a) Fluorescence spectra of rhodamine-B-labelled quasi-block copolymers at 10 µg/mL in $CHCl_3$. **(b)** FACS plots showing the fluorescence intensity of rhodamine in $CD206^+$ primary murine macrophages after incubation with glycosylated copolymers (10 µg/mL) (gating given in the ESI). Mannose- and galactose-based copolymers have a similar fluorescence intensity, however the normalized flow cytometric value suggests that mannose-based copolymers are taken up at least two-fold more efficiently than the polymers with galactose. Polymers used were from batch synthesis post-ChemSpeed: ManMA = mannose-based copolymer: = P(BMA-*co*-MAA-*qb*-NMS-*qb*-PEGMA-*co*-ManMA - (M_n = 14.5 kDa, $Đ$ = 1.55)); GalMA = galactose-based copolymer: P(BMA-*co*-MAA-*qb*-NMS-*qb*-PEGMA-*co*-GalMA)(M_n = 13.5 kDa, $Đ$ = 1.54); no sugar polymer: P(BMA-*co*-MAA-*qb*-NMS-*qb*-PEGMA).

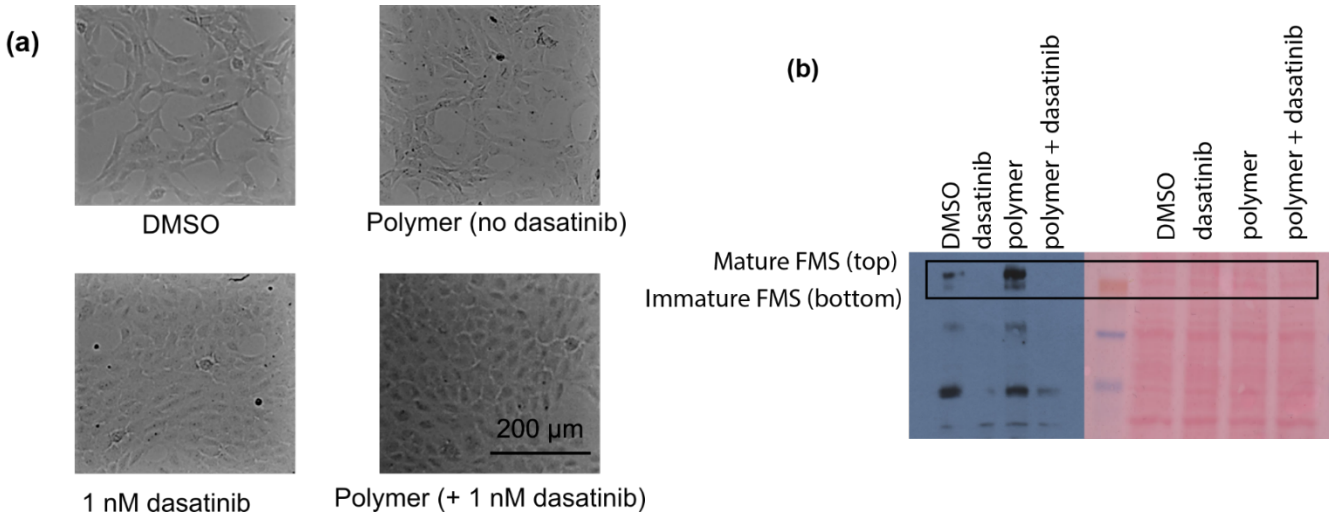

Figure 6 (a) Rat-2 vfms fibroblasts after treatment with dasatinib (1 nM) and dasatinib-loaded : P(BMA-*co*-MAA-*qb*-NMS-*qb*-PEGMA-*co*-ManMA nanoparticles (1 nM confirmed concentration of dasatinib post-dialysis and lyophilization) for 2 h. A clear morphology change is observed compared to the controls. The DMSO-treated control cells have the same morphology as untreated cells.[9] Scale bar = 200 µm. **(b)** Western blot to show the successful inhibition of FMS with the glycosylated drug delivery vehicles *via* disappearance of the mature FMS and immature FMS bands. D = free dasatinib (1 nM), P = copolymer with no drug loaded, P+D = copolymer with 1 nM dasatinib loaded. The full blot can be found in the SI (**Figure S33**).

to terminal mannose residues on pathogens and is able to mediate phagocytosis and pinocytosis of particles containing mannose.[60] Primary murine macrophages were selected as an initial model to assess uptake *via* CD206.[61,62] The cells were isolated from the peritoneal cavity of mice and were incubated with glycosylated P(BMA-*co*-MAA-*qb*-NMS-*qb*-PEGMA) copolymers. They were then analyzed by flow cytometry, following immunostaining. The cellular markers Mac-1 and F4/80 were used to differentiate macrophages from non-macrophages.[63] Uptake was then assessed by analyzing the fluorescence intensity of RhoB (582 nm).

The role of CD206 for uptake was initially investigated by pre-treating the macrophages with mannose (50 mM) to saturate the receptor, before incubating with polymer (10 µg/mL). [64] Initial polymer incubation was carried out at 0 °C for 30 min to minimize endocytosis and maximize receptor binding. The cells were then warmed to room temperature for 5 min and excess polymer was washed away. The results are summarized in **Figure 4.** Polymers with exposed mannose on the outer shell had a lower uptake relative to untreated cells. A 25% decrease in mean fluorescence intensity (MFI) was observed. Polymers with galactose and polymers with no glycomonomer showed only minimal decrease. These results are expected if the uptake of the mannose-bearing nanoparticles is (at least in part) reliant on CD206 for uptake. This effect has also been observed by Huang and co-workers.[64]

As further confirmation of the role of CD206 in uptake, primary macrophages were immunolabelled with anti-mouse CD206 (MMR) antibody (**Figure 5**). Cells were gated on $Mac1^{+}F4/80^{+}$ markers and expression of CD206 was analyzed against rhodamine intensity. It would be expected that cells with a higher level of CD206 show an increased uptake of particles bearing mannose units. **Figure 5(a)** shows the fluorescence spectra of the polymers at 10 µg/mL in $CHCl_3$, which was used to qualitatively compare the rhodamine loading of each polymer composition (it should be noted that $CHCl_3$ was used for normalization to avoid any differences in fluorescence that would be observed by micelle formation and aggregation; all three polymers were fully soluble in $CHCl_3$, which allowed for direct fluorescence measurements for each concentration of polymer). This allows normalization of the flow cytometry data (**Figure 5(b)**) against the intrinsic fluorescence signal of the particles. Normalization can be done by dividing the MFI (flow cytometry) by the maximum emission (fluorescence spectroscopy). From this normalization process, the GalMA-based copolymer and polymer without sugar had an efficiency index of ~55, whereas the mannose-based copolymer had an efficiency index of ~106. This further demonstrates the importance of CD206 in the uptake of these materials, however, does not rule out non-specific uptake by macrophages. We also cannot discount the role that polymer negative charge may have on the uptake. This will be a subject of future studies.

Impact of dasatinib-loaded nanoparticles

To determine whether the drug-loaded micelles were releasing their cargo to engage the FMS receptor, an uptake study was carried out with Rat-2 fibroblasts that express the v-fms oncogene.[9] When these cells express v-fms they have a transformed morphology as shown in **Figure 6(a)**. [65] When FMS was suppressed by dasatinib (1 nM) there was a clear morphology change from spindle-like and disordered to more uniform and globular. The same effect was observed with cells that were treated with dasatinib-loaded P(BMA-*co*-MAA-*b*-NMS-*co*-

PEGMA-*qb*-ManMA) copolymers for 2 h. These cells were then lysed and quantified *via* Western blotting (**Figure 6(b)**). This data shows the clear inhibitory effect that dasatinib (D), and consequently the dasatinib-loaded nanoparticles (P+D), has on FMS signaling in the fibroblast cell line relative to the polymer with no dasatinib (P) and the vehicle (DMSO). It should be noted that, based on the drug-leakage study, <18% of the total concentration of dasatinib would have leaked out into the surrounding media (timepoint taken for leakage study: 6 h = 18% leakage into surrounding media; time point taken for this experiment = 2 h). This corresponds to a concentration < 180 pM, which is below the concentration required to induce a morphology change in these cells (approximately 500 pM).[9] This therefore demonstrates the success of our drug delivery system for FMS inhibitor delivery to cells.

Conclusions

A series of fluorescently labelled, glycosylated quasi-block copolymers were synthesized with varied ratios of hydrophobic and hydrophilic blocks. These compositions were then assembled into nanoparticles, cross-linked and loaded with the kinase inhibitor dasatinib. *In vitro* studies showed that these nanoparticles were successfully internalized into macrophages, in part, *via* the macrophage mannose receptor (CD206). Furthermore, we were able to demonstrate successful delivery of dasatinib to cells using this system, resulting in inhibition of the FMS receptor. As such, this study lays the groundwork for further drug delivery studies aimed at specifically targeting TAMs with molecularly targeted therapeutics.

AUTHOR INFORMATION

Corresponding Author

Professor Matthew J. Fuchter, Molecular Sciences Research Hub, Department of Chemistry, Imperial College London, White City Campus, London, UK, W12 0BZ.

Email: m.fuchter@imperial.ac.uk

Author Contributions

All authors have given approval to the final version of the manuscript.

Funding Sources

Funding for this work was provided by the Commonwealth Scientific and Industrial Research Organization (CSIRO) and Imperial College London. MJF would like to thank the EPSRC for an Established Career Fellowship (EP/R00188X/1).

ACKNOWLEDGMENT

We would like to thank Dr Ben Muir and Dr Shaun Howard for help with the ChemSpeed experiments, Jess Hatwell-Humble for animal assistance, Peter Haycock and Roger Mulder for NMR assistance, Dr Lisa Haigh for mass spectrometry assistance, Mark Hickey and Lisa Famularo for GPC assistance and finally Jacinta White for cryo-TEM assistance.

SUPPORTING INFORMATION

Preparation and characterization of all monomers and polymers used in this work, as well as other supplementary figures. Methods used in biological studies.

REFERENCES

(1) Morrison, C. Immuno-Oncologists Eye up Macrophage Targets. *Nat. Rev. Drug Discov.* **2016**, *15* (6), 373–374.

(2) Ngambenjawong, C.; Gustafson, H. H.; Pun, S. H. Progress in Tumor-Associated Macrophage (TAM)-Targeted Therapeutics. *Adv. Drug Deliv. Rev.* **2017**, *114*, 206–221.

(3) Ginhoux, F.; Jung, S. Monocytes and Macrophages: Developmental Pathways and Tissue Homeostasis. *Nat. Rev. Immunol.* **2014**, *14* (6), 392–404.

(4) Pollard, J. W. Tumour-Educated Macrophages Promote Tumour Progression and Metastasis. *Nat. Rev. Cancer* **2004**, *4* (1), 71–78.

(5) Mantovani, A.; Marchesi, F.; Malesci, A.; Laghi, L.; Allavena, P. Tumour-Associated Macrophages as Treatment Targets in Oncology. *Nat. Rev. Clin. Oncol.* **2017**, *14* (7), 399–416.

(6) El-Gamal, M. I.; Anbar, H. S.; Yoo, K. H.; Oh, C.-H. FMS Kinase Inhibitors: Current Status and Future Prospects. *Med. Res. Rev.* **2013**, *33* (3), 599–636.

(7) van Dalen, F.; van Stevendaal, M.; Fennemann, F.; Verdoes, M.; Ilina, O. Molecular Repolarisation of Tumour-Associated Macrophages. *Molecules* **2018**, *24* (1), 9.

(8) Olmos-Alonso, A.; Schetters, S. T. T.; Sri, S.; Askew, K.; Mancuso, R.; Vargas-Caballero, M.; Holscher, C.; Perry, V. H.; Gomez-Nicola, D. Pharmacological Targeting of CSF1R Inhibits Microglial Proliferation and Prevents the Progression of Alzheimer's-like Pathology. *Brain* **2016**, *139* (3), 891–907.

(9) Brownlow, N.; Mol, C.; Hayford, C.; Ghaem-Maghami, S.; Dibb, N. J. Dasatinib Is a Potent Inhibitor of Tumour-Associated Macrophages, Osteoclasts and the FMS Receptor. *Leukemia* **2009**, *23* (3), 590–594.

(10) Hoehn, D.; Cortes, J. E.; Medeiros, L. J.; Jabbour, E. J.; Hidalgo, J. E.; Kanagal-Shamanna, R.; Bueso-Ramos, C. E. Multiparameter Analysis of Off-Target Effects of Dasatinib on Bone Homeostasis in Patients With Newly Diagnosed Chronic Myelogenous Leukemia. *Clin. Lymphoma, Myeloma Leuk.* **2016**, *16* (August), S86–S92.

(11) Kawakami, S.; Sato, A.; Nishikawa, M.; Yamashita, F.; Hashida, M. Mannose Receptor-Mediated Gene Transfer into Macrophages Using Novel Mannosylated Cationic Liposomes. *Gene Ther.* **2000**, *7* (4), 292–299.

(12) Clemens, D. L.; Lee, B.-Y.; Xue, M.; Thomas, C. R.; Meng, H.; Ferris, D.; Nel, A. E.; Zink, J. I.; Horwitz, M. A. Targeted Intracellular Delivery of Antituberculosis Drugs to Mycobacterium Tuberculosis-Infected Macrophages via Functionalized Mesoporous Silica Nanoparticles. *Antimicrob. Agents Chemother.* **2012**, *56* (5), 2535–2545.

(13) Zhang, F.; Mastorakos, P.; Mishra, M. K.; Mangraviti, A.; Hwang, L.; Zhou, J.; Hanes, J.; Brem, H.; Olivi, A.; Tyler, B.; Kannan, R. M. Uniform Brain Tumor Distribution and Tumor Associated Macrophage Targeting of Systemically Administered Dendrimers. *Biomaterials* **2015**, *52*, 507–516.

(14) VanHandel, M.; Alizadeh, D.; Zhang, L.; Kateb, B.; Bronikowski, M.; Manohara, H.; Badie, B. Selective Uptake of Multi-Walled Carbon Nanotubes by Tumor Macrophages in a Murine Glioma Model. *J. Neuroimmunol.* **2009**, *208* (1–2), 3–9.

(15) Ortega, R. A.; Barham, W.; Sharman, K.; Tikhomirov, O.; Giorgio, T. D.; Yull, F. E. Manipulating the NF-KB Pathway in Macrophages Using Mannosylated, SiRNA-Delivering Nanoparticles Can Induce Immunostimulatory and Tumor Cytotoxic Functions. *Int. J. Nanomedicine* **2016**, *11*, 2163–2177.

(16) Ortega, R. A.; Barham, W. J.; Kumar, B.; Tikhomirov, O.; McFadden, I. D.; Yull, F. E.; Giorgio, T. D. Biocompatible

Mannosylated Endosomal-Escape Nanoparticles Enhance Selective Delivery of Short Nucleotide Sequences to Tumor Associated Macrophages. *Nanoscale* **2015**, *7* (2), 500–510.

(17) Kedar, U.; Phutane, P.; Shidhaye, S.; Kadam, V. Advances in Polymeric Micelles for Drug Delivery and Tumor Targeting. *Nanomedicine Nanotechnology, Biol. Med.* **2010**, *6* (6), 714–729.

(18) Liao, Z. S.; Huang, S. Y.; Huang, J. J.; Chen, J. K.; Lee, A. W.; Lai, J. Y.; Lee, D. J.; Cheng, C. C. Self-Assembled PH-Responsive Polymeric Micelles for Highly Efficient, Noncytotoxic Delivery of Doxorubicin Chemotherapy to Inhibit Macrophage Activation: In Vitro Investigation. *Biomacromolecules* **2018**, *19* (7), 2772–2781.

(19) Yu, S. S.; Lau, C. M.; Barham, W. J.; Onishko, H. M.; Nelson, C. E.; Li, H.; Smith, C. A.; Yull, F. E.; Duvall, C. L.; Giorgio, T. D. Macrophage-Specific RNA Interference Targeting via "Click", Mannosylated Polymeric Micelles. *Mol. Pharm.* **2013**, *10* (3), 975–987.

(20) Karabin, N. B.; Allen, S.; Kwon, H.-K.; Bobbala, S.; Firlar, E.; Shokuhfar, T.; Shull, K. R.; Scott, E. A. Sustained Micellar Delivery via Inducible Transitions in Nanostructure Morphology. *Nat. Commun.* **2018**, *9* (1), 624.

(21) Murdoch, C; Reeves, K, J; Hearnden, V; Colley, H; Massignani, M; Canton, I; Madsen, J; Blanazs, A; Armes, S.P; Lewis, A; MacNeil, S; Brown, N; Thornhill, M; Battaglia, G. Internalization and Biodistribution of Polymersomes into Oral Squamous Cell Carcinoma Cells in Vitro and in Vivo The. *Nanomedicine* **2006**, *20* (21), 1335–1342.

(22) Eissa, A. M.; Smith, M. J. P.; Kubilis, A.; Mosely, J. A.; Cameron, N. R. Polymersome-Forming Amphiphilic Glycosylated Polymers : Synthesis and Characterization. *J. Polym. Sci. Part A Polym. Chem.* **2013**, *51*, 5184–5193.

(23) Praphakar, R. A.; Shakila, H.; Azger Dusthackeer, V. N.; Munusamy, M. A.; Kumar, S.; Rajan, M. A Mannose-Conjugated Multi-Layered Polymeric Nanocarrier System for Controlled and Targeted Release on Alveolar Macrophages. *Polym. Chem.* **2018**, *9* (5), 656–667.

(24) Das, D.; Srinivasan, S.; Brown, F. D.; Su, F. Y.; Burrell, A. L.; Kollman, J. M.; Postma, A.; Ratner, D. M.; Stayton, P. S.; Convertine, A. J. Radiant Star Nanoparticle Prodrugs for the Treatment of Intracellular Alveolar Infections. *Polym. Chem.* **2018**, *9* (16), 2134–2146.

(25) Zhu, S.; Niu, M.; O'Mary, H.; Cui, Z. Targeting of Tumor-Associated Macrophages Made Possible by PEG-Sheddable, Mannose-Modified Nanoparticles. *Mol. Pharm.* **2013**, *10* (9), 3525–3530.

(26) Dag, A.; Zhao, J.; Stenzel, M. H. Origami with ABC Triblock Terpolymers Based on Glycopolymers: Creation of Virus-Like Morphologies. *ACS Macro Lett.* **2015**, *4* (5), 579–583.

(27) Su, F.; Srinivasan, S.; Lee, B.; Chen, J.; Convertine, A. J.; Eoin, T.; Ratner, D. M.; Skerrett, S. J.; Stayton, P. S. Macrophage-Targeted Drugamers with Enzyme-Cleavable Linkers Deliver High Intracellular Drug Dosing and Sustained Drug Pharmacokinetics against Alveolar Pulmonary Infections. *J. Control. Release* **2018**, *287* (May), 1–11.

(28) Moad, G.; Rizzardo, E.; Thang, S. H. Living Radical Polymerization by the RAFT Process—A First Update. *Aust. J. Chem.* **2006**, *59* (10), 669.

(29) Moad, G.; Rizzardo, E.; Thang, S. H. Living Radical Polymerization by the RAFT Process—A Second Update. *Aust. J. Chem.* **2009**, *59* (10), 669.

(30) Guerrero-Sanchez, C.; O'Brien, L.; Brackley, C.; Keddie, D. J.; Saubern, S.; Chiefari, J. Quasi-Block Copolymer Libraries on Demand via Sequential RAFT Polymerization in an Automated Parallel Synthesizer. *Polym. Chem.* **2013**, *4* (6), 1857.

(31) Montgomery, K. S.; Davidson, R. W. M.; Cao, B.; Williams, B.; Simpson, G. W.; Nilsson, S. K.; Chiefari, J.; Fuchter, M. J. Effective Macrophage Delivery Using RAFT Copolymer Derived Nanoparticles. *Polym. Chem.* **2018**, *9*, 131–137.

(32) Cao, H.; Dong, Y.; Bre, L.; Tapeinos, C.; Wang, W.; Pandit, A. An Acetal-Based Polymeric Crosslinker with Controlled PH-Sensitivity. *RSC Adv.* **2016**, *6* (12), 9604–9611.

(33) Chiefari, J.; Chong, Y. K. B.; Ercole, F.; Krstina, J.; Jeffery, J.; Le, T. P. T.; Mayadunne, R. T. A.; Meijs, G. F.; Moad, C. L.; Moad, G.; Rizzardo, E.; Thang, S. H. Living Free-Radical Polymerization by Reversible Addition−Fragmentation Chain Transfer: The RAFT Process. *Macromolecules* **1998**, *31* (16), 5559–5562.

(34) Chaduc, I.; Crepet, A.; Boyron, O.; Charleux, B.; D'Agosto, F.; Lansalot, M. Effect of the Ph on the Raft Polymerization of Acrylic Acid in Water. Application to the Synthesis of Poly(Acrylic Acid)-Stabilized Polystyrene Particles by RAFT Emulsion Polymerization. *Macromolecules* **2013**, *46* (15), 6013–6023.

(35) Ji, J.; Jia, L.; Yan, L.; Bangal, P. R. Efficient Synthesis of Poly(Acrylic Acid) in Aqueous Solution via a RAFT Process. *J. Macromol. Sci. Part A Pure Appl. Chem.* **2010**, *47* (5), 445–451.

(36) Muthukrishnan, S.; Pan, E. H.; Stenzel, M. H.; Barner-Kowollik, C.; Davis, T. P.; Lewis, D.; Barner, L. Ambient Temperature RAFT Polymerization of Acrylic Acid Initiated with Ultraviolet Radiation in Aqueous Solution. *Macromolecules* **2007**, *40* (9), 2978–2980.

(37) Tiwari, N.; Badiger, M. V. Enhanced Drug Release by Selective Cleavage of Cross-Links in a Double-Cross-Linked Hydrogel. *RSC Adv.* **2016**, *6* (104), 102453–102461.

(38) Xu, L.; Zhu, Y.; Chen, L.; An, H.; Zhang, W.; Wang, G.; Lin, Z.; Xu, J. Prognostic Value of Diametrically Polarized Tumor-Associated Macrophages in Renal Cell Carcinoma. *Ann. Surg. Oncol.* **2014**, *21* (9), 3142–3150.

(39) Scodeller, P.; Simón-Gracia, L.; Kopanchuk, S.; Tobi, A.; Kilk, K.; Säälik, P.; Kurm, K.; Squadrito, M. L.; Kotamraju, V. R.; Rinken, A.; De Palma, M.; Ruoslahti, E.; Teesalu, T. Precision Targeting of Tumor Macrophages with a CD206 Binding Peptide. *Sci. Rep.* **2017**, *7* (1), 1–12.

(40) Boskovic, J.; Arnold, J. N.; Stilion, R.; Gordon, S.; Sim, R. B.; Rivera-Calzada, A.; Wienke, D.; Isacke, C. M.; Martinez-Pomares, L.; Llorca, O. Structural Model for the Mannose Receptor Family Uncovered by Electron Microscopy of Endo180 and the Mannose Receptor. *J. Biol. Chem.* **2006**, *281* (13), 8780–8787.

(41) Lundquist, J. J.; Toone, E. J. The Cluster Glycoside Effect. *Chem. Rev.* **2002**, *102*, 555–578.

(42) Ambrosi, M.; Cameron, N. R.; Davis, B. G. Lectins: Tools for the Molecular Understanding of the Glycocode. *Org. Biomol. Chem.* **2005**, *3* (9), 1593–1608.

(43) Lee, Y. C.; Lee, R. T. Carbohydrate-Protein Interactions: Basis of Glycobiology. *Acc. Chem. Res.* **1995**, *28* (8), 321–327.

(44) Wang, Y.; Li, X. I. N.; Hong, C.; Pan, C. Synthesis and Micellization of Thermoresponsive Galactose-Based Diblock Copolymers. *J. Polym. Sci. Part A Polym. Chem.* **2011**, *49*, 3280–3290.

(45) Pomposo, J. A.; Perez-Baena, I.; Buruaga, L.; Alegría, A.; Moreno, A. J.; Colmenero, J. On the Apparent SEC Molecular Weight and Polydispersity Reduction upon Intramolecular Collapse of Polydisperse Chains to Unimolecular Nanoparticles. *Macromolecules* **2011**, *44* (21), 8644–8649.

(46) Pomposo, J. A.; Perez-Baena, I.; Lo Verso, F.; Moreno, A. J.; Arbe, A.; Colmenero, J. How Far Are Single-Chain Polymer Nanoparticles in Solution from the Globular State? *ACS Macro Lett.* **2014**, *3* (8), 767–772.

(47) Whitaker, D. E.; Mahon, C. S.; Fulton, D. A. Thermoresponsive Dynamic Covalent Single-Chain Polymer Nanoparticles Reversibly Transform into a Hydrogel. *Angew. Chemie* **2013**, *125* (3), 990–993.

(48) Liang, Y.; Li, Z.-C.; Chen, G.; Li, F. Synthesis of Well-Defined Poly[(2-β-D-Glucopyranosyloxy)Ethyl Acrylate] by Atom Transfer Radical Polymerization. *Polym. Int.* **1999**, *48* (9), 739–742.

(49) Haddleton, D. M.; Ohno, K. Well-Defined Oligosaccharide-Terminated Polymers from Living Radical Polymerization. *Biomacromolecules* **2000**, *1* (2), 152–156.

(50) Pfaff, A.; Shinde, V. S.; Lu, Y.; Wittemann, A.; Ballauff, M.; Müller, A. H. E. Glycopolymer-Grafted Polystyrene Nanospheres. *Macromol. Biosci.* **2011**, *11* (2), 199–210.

(51) Shi, H.; Liu, L.; Wang, X.; Li, J. Glycopolymer-Peptide Bioconjugates with Antioxidant Activity via RAFT Polymerization. *Polym. Chem.* **2012**, *3* (5), 1182–1188.

(52) Zhou, D.; Li, C.; Hu, Y.; Zhou, H.; Chen, J.; Zhang, Z.; Guo, T. Glycopolymer Modification on Physicochemical and Biological Properties of Poly(l-Lysine) for Gene Delivery. *Int. J. Biol. Macromol.* **2012**, *50* (4), 965–973.

(53) Dan, K.; Ghosh, S. PH-Responsive Aggregation of Amphiphilic Glyco-Homopolymer. *Macromol. Rapid Commun.* **2012**, *33* (2), 127–132.

(54) Simon Ting, S. R.; Gregory, A. M.; Stenzel, M. H. Polygalactose Containing Nanocages: The Raft Process for the Synthesis of Hollow Sugar Balls. *Biomacromolecules* **2009**, *10* (2), 342–352.

(55) Colombani, O.; Ruppel, M.; Schubert, F.; Zettl, H.; Pergushov, D. V; Mu, A. H. E.; Müller, A. H. E. Synthesis Pf PBA-b-PAA Diblock Copolymers by ATRP and Their Micellization in Water. *Macromolecules* **2007**, *40*, 4338–4350.

(56) Dreher, M. R.; Liu, W.; Michelich, C. R.; Dewhirst, M. W.; Yuan, F.; Chilkoti, A. Tumor Vascular Permeability, Accumulation, and Penetration of Macromolecular Drug Carriers. *J. Natl. Cancer Inst.* **2006**, *98* (5), 335–344.

(57) Fox, M.; Szoka, F. C.; Frechet, M. J. Importance of Molecular Architecture. *Acc Chem Res.* **2010**, *42* (8), 1141–1151.

(58) Mirshafiee, V.; Kim, R.; Mahmoudi, M.; Kraft, M. L. The Importance of Selecting a Proper Biological Milieu for Protein Corona Analysis in Vitro: Human Plasma versus Human Serum. *Int. J. Biochem. Cell Biol.* **2016**, *75*, 188–195.

(59) Li, S. D.; Huang, L. Stealth Nanoparticles: High Density but Sheddable PEG Is a Key for Tumor Targeting. *J. Control. Release* **2010**, *145* (3), 178–181.

(60) Taylor, E.; Conarytn, J. T.; Lennartz, R.; Stahl, D.; Parker, I.; Francis, B. Primary Structure of the Mannose Receptor Contains Multiple Resembling Carbohydrate-Recognition Domains *. *J. Biol. Chem.* **1990**, *265* (21), 12156–12162.

(61) Wang, C.; Yu, X.; Cao, Q.; Wang, Y.; Zheng, G.; Tan, T. K.; Zhao, H.; Zhao, Y.; Wang, Y.; Harris, D. C. H. Characterization of Murine Macrophages from Bone Marrow, Spleen and Peritoneum. *BMC Immunol.* **2013**, *14* (1), 6.

(62) Bisgaard, L. S.; Mogensen, C. K.; Rosendahl, A.; Cucak, H.; Nielsen, L. B.; Rasmussen, S. E.; Pedersen, T. X. Bone Marrow-Derived and Peritoneal Macrophages Have Different Inflammatory Response to OxLDL and M1/M2 Marker Expression – Implications for Atherosclerosis Research. *Sci. Rep.* **2016**, *6* (1), 35234.

(63) Inoue, Tsutomu; Plieth, David; Venkov, Christo; Xu, Carol; Neilson, E. Antibodies against Macrophages That Overlap in Specificity with Fibroblasts. *Kidney Int.* **2005**, *67*, 2488–2493.

(64) Zhao, P.; Yin, W.; Wu, A.; Tang, Y.; Wang, J.; Pan, Z.; Lin, T.; Zhang, M.; Chen, B.; Duan, Y.; Huang, Y. Dual-Targeting to Cancer Cells and M2 Macrophages via Biomimetic Delivery of Mannosylated Albumin Nanoparticles for Drug-Resistant Cancer Therapy. *Adv. Funct. Mater.* **2017**, *27* (44), 1–15.

(65) Taylor, J. R.; Brownlow, N.; Domin, J.; Dibb, N. J. FMS Receptor for M-CSF (CSF-1) Is Sensitive to the Kinase Inhibitor Imatinib and Mutation of Asp-802 to Val Confers Resistance. *Oncogene* **2006**, *25*, 147–151.

TOC artwork